DOI: https://doi.org/10.15407/pmach2025.04.062

UDC 621.316.11

DEVELOPMENT OF RENEWABLE ENERGY SYSTEM USING A DISTRIBUTED SLACK BUS MODEL

Muhanned Al-Rawi
muhrawi@yahoo.com
ORCID: 0000-0003-1407-6519

Bandung Institute of Technology,
Jalan Ganesa No. 10, Coblong, Kota Bandung, Jawa Barat, Indonesia 40132

In this study, a distributed slack bus (DSB) approach utilizing combined participation factors, which are based on the scheduled generation capacities of the system, has been developed to allocate system losses among the generators. A DSB algorithm has been created and executed using a Newton Raphson solver within the MATLAB environment. The IEEE 14 bus system serves as a case study for this research. Renewable energy sources are integrated into the system, and a comparative analysis of the generation costs is conducted between systems incorporating renewable energy sources and those relying solely on thermal generators, evaluated through both the single slack bus (SSB) model and the DSB model. The implementation of the DSB led to a decrease in overall real power generation, reducing it from 272.593 MW to 272.409 MW in the 14 bus system, alongside a reduction in generation costs across both bus types. Additionally, real power line losses were minimized. The alterations in generation levels of the voltage-controlled buses fostered an effective economic dispatch scheme, accurately reflecting the network parameters. The introduction of wind and solar generators significantly lowered the cost of generation compared to systems devoid of these resources. Furthermore, employing combined participation factors yielded an even more precise network model.

Keywords: *distributed slack bus, renewable energy, economic dispatch, power.*

Introduction

Economic dispatch involves the strategic allocation of the total load across generating units that function simultaneously within a power system. This process is grounded in two key principles: first, that the generating units must meet the power system's load requirements while minimizing costs through optimal unit utilization. Second, these units must remain capable of providing backup support in case of failures in other units, all while adhering to specified constraints.

The slack bus refers to the component that supplies additional real and reactive power to address transmission losses within the power system. It also serves as a reference point for the measurement of voltage magnitude and phase angle [1–4].

Implementation of a distributed slack bus model offers means for alleviating the concentrated demands placed on a single slack bus by redistributing losses among each generator bus in the power system. This enables the system's generators to adjust their outputs in accordance with their operational limits, promoting economic efficiency. This model was developed to overcome the limitations associated with the traditional single slack bus model, which does not reflect the realities of modern power systems. The need for this approach has been amplified by the rise in distributed generation along with the deregulation and liberalization trends in the power generation sector [5–7].

Renewable energy refers to energy sourced from natural processes that are continuously replenished, allowing for the production of usable energy forms. Examples of these sources include solar, wind, hydro, geothermal, and biomass ones. This study particularly focuses on two types of renewable energy: wind and solar ones.

Wind energy is a fundamentally different manifestation of solar energy. The sun’s rays impact the Earth's surface, warming the air above oceans and land masses, which leads to the formation of wind currents. Humanity has relied on wind for millennia, initially using it to navigate ships across the seas, and later – for purposes such as water pumping and grain milling. In contemporary times, wind energy has emerged as a clean and dependable source of electricity.

With solar energy being widely available throughout the nation, it is rightly regarded as a primary resource for exploitation. While it primarily serves as a supplementary energy source, it also plays a vital role in mitigating atmospheric pollution and combating climate change.

1 Design methodology

1.1 Formation of the improved Newton Raphson matrix

The chosen distributed slack bus (DSB) model incorporates a participation factor that depends on the actual power generation occurring at generator buses. By utilizing a Newton-Raphson solver with this participation factor, the conventional Newton-Raphson matrix is modified. Specifically, the modifications involve reclassifying the slack bus as a generator bus, thereby including it in the Jacobian matrix, along with the introduction of a participation factor. This leads to the creation of a matrix referred to as the extended Jacobian (J_e). Consequently, the Jacobian matrix no longer retains its symmetry, and its new dimensions are expressed as $(2n\text{-}m)\times(2n\text{-}m\text{-}1)$, where n represents the total number of buses in the system, and m denotes the number of generator buses. Furthermore, a term for real power loss (P_{loss}), which is multiplied by the participation factors, is also integrated into the corrections matrix. As a result, the total real power (P) injection within the system is altered accordingly, as follows

$$P_i = \sum_{k=1}^{n} |V_i| \cdot |V_k| \cdot |Y_{ik}| \cos(\theta_{ik} + \delta_k - \delta_i) + K_i(i) \cdot P_{loss},$$

where V_i is the voltage at the i-th bus; V_k is the voltage at the k-th bus; Y_{ik} is the admittance; δ is the voltage angle; K_i is participation factor.

The reactive power (Q_i) equation remains similar to the single slack bus model since it does not depend on the selected participation factor and is given by

$$Q_i = -\sum_{k=1}^{n} |V_i| \cdot |V_k| \cdot |Y_{ik}| \sin(\theta_{ik} + \delta_k - \delta_i).$$

The ordinary NR matrix thus changes as shown below

$$\begin{vmatrix} \Delta P_1 \\ \vdots \\ \Delta P_n \\ \hline \Delta Q_1 \\ \vdots \\ \Delta Q_{n-m} \end{vmatrix} = \left| \begin{array}{ccc|ccc} \left(\frac{\partial P_1}{\partial \delta_1}\right) & \cdots & \left(\frac{\partial P_2}{\partial \delta_n}\right) & \left(\frac{\partial P_1}{\partial |V_1|}\right) & \cdots & \left(\frac{\partial P_1}{\partial |V_{n-m}|}\right) & K_i \\ \vdots & \ddots & \vdots & \vdots & \ddots & \vdots & \vdots \\ \left(\frac{\partial P_n}{\partial \delta_1}\right) & \cdots & \left(\frac{\partial P_n}{\partial \delta_n}\right) & \left(\frac{\partial P_n}{\partial |V_1|}\right) & \cdots & \left(\frac{\partial P_n}{\partial |V_{n-m}|}\right) & K_n \\ \hline \left(\frac{\partial Q_1}{\partial \delta_1}\right) & \cdots & \left(\frac{\partial Q_1}{\partial \delta_n}\right) & \left(\frac{\partial Q_2}{\partial |V_1|}\right) & \cdots & \left(\frac{\partial Q_1}{\partial |V_{n-m}|}\right) & \frac{\partial Q_1}{\partial P_{loss}} \\ \vdots & \ddots & \vdots & \vdots & \ddots & \vdots & \vdots \\ \left(\frac{\partial Q_{n-m}}{\partial \delta_1}\right) & \cdots & \left(\frac{\partial Q_{n-m}}{\partial \delta_n}\right) & \left(\frac{\partial Q_{n-m}}{\partial |V_1|}\right) & \cdots & \left(\frac{\partial Q_{n-m}}{\partial |V_{n-m}|}\right) & \frac{\partial Q_1}{\partial P_{loss}} \end{array} \right| \cdot \begin{vmatrix} \Delta\delta_1 \\ \vdots \\ \Delta\delta_n \\ \Delta|V_1| \\ \vdots \\ \Delta|V_{n-m}| \\ \Delta P_{loss} \end{vmatrix}.$$

Since the selected participation factor depends only on real powers, some terms in the extended Jacobian matrix above are removed.

For real power in the generator buses, $\frac{\partial P_i}{\partial P_{loss}} = K_i$, which represents our participation factors. For the load buses, $\frac{\partial P_i}{\partial P_{loss}} = 0$. The reactive powers are not included in the participation factors. The resulting extended Jacobian matrix is thus reduced as shown below

$$\begin{vmatrix} \Delta P_1 \\ \vdots \\ \Delta P_n \\ \hline \Delta Q_1 \\ \vdots \\ \Delta Q_{n-m} \end{vmatrix} = \left| \begin{array}{ccc|ccc} \left(\frac{\partial P_1}{\partial \delta_1}\right) & \cdots & \left(\frac{\partial P_2}{\partial \delta_n}\right) & \left(\frac{\partial P_1}{\partial |V_1|}\right) & \cdots & \left(\frac{\partial P_1}{\partial |V_{n-m}|}\right) & K_i \\ \vdots & \ddots & \vdots & \vdots & \ddots & \vdots & \vdots \\ \left(\frac{\partial P_n}{\partial \delta_1}\right) & \cdots & \left(\frac{\partial P_n}{\partial \delta_n}\right) & \left(\frac{\partial P_n}{\partial |V_1|}\right) & \cdots & \left(\frac{\partial P_n}{\partial |V_{n-m}|}\right) & K_m \\ \hline \left(\frac{\partial Q_1}{\partial \delta_1}\right) & \cdots & \left(\frac{\partial Q_1}{\partial \delta_n}\right) & \left(\frac{\partial Q_2}{\partial |V_1|}\right) & \cdots & \left(\frac{\partial Q_1}{\partial |V_{n-m}|}\right) & 0 \\ \vdots & \ddots & \vdots & \vdots & \ddots & \vdots & \vdots \\ \left(\frac{\partial Q_{n-m}}{\partial \delta_1}\right) & \cdots & \left(\frac{\partial Q_{n-m}}{\partial \delta_n}\right) & \left(\frac{\partial Q_{n-m}}{\partial |V_1|}\right) & \cdots & \left(\frac{\partial Q_{n-m}}{\partial |V_{n-m}|}\right) & 0 \end{array} \right| \cdot \begin{vmatrix} \Delta\delta_1 \\ \vdots \\ \Delta\delta_n \\ \Delta|V_1| \\ \vdots \\ \Delta|V_{n-m}| \\ \Delta P_{loss} \end{vmatrix}.$$

1.2 Formulation of fuel cost functions

For thermal generator, it is required to minimize the fuel cost with real power output. This can be done below.

The fuel cost function of each fossil fuel fired generator is expressed as a quadratic function. The total fuel cost in terms of real power output can be expressed as

$$C(P_{gi}) = \sum_{i=1}^{NG} \left(a_i P_{gi}^2 + b_i P_{gi} + c_i \right),$$

where a_i, b_i and c_i are the fuel cost coefficients of i-th unit; NG is the number of generators; P_{gi} is active generator or real power.

The reduction of fuel costs through the management of reactive power output is also achievable. The cost associated with reactive power generation is significantly influenced by the output of real power. When a generator operates at its maximum active power ($P^{\max}$), it does not generate any reactive power. Consequently, the apparent power is equivalent to $P^{\max}$, and any generation of reactive power will lead to a decrease in the production of active power.

To generate reactive power (Q_{gi}) from a generator (I), it is necessary to lower its active power to P_{gi}. Thus, for varying values of Q_{gi} in relation to P_{gi}, the quadratic cost function for reactive power is determined by fitting a curve to a quadratic polynomial. The fuel cost, in terms of reactive power output, can be articulated as follows

$$C(Q_{gi}) = \sum_{i=1}^{NG} \left(a_{gi} Q_{gi}^2 + b_{gi} + c_{gi} \right),$$

where a_{gi}, b_{gi}, c_{gi} are reactive power cost coefficients, calculated using a curve fitting; NG is number of generators.

Furthermore, the operating cost function of the wind farm can be obtained. The linear cost function assumed for the wind farm is given as follows:

$$C_{wi}(W_i) = d_i W_i,$$

where d_i is direct cost coefficient of i-th wind farm; W_i is actual wind power.

For cost junction due to the over-generation, the penalty cost caused by not using all the available wind power is related to the difference between the available wind power and the actual wind power used. The mathematical model is written as follows

$$C_{pwi}(W_{iav} - W_i) = K_{pi}(W_{iav} - W_i) = K_{pi}\left\{(W - W_i) f_w(W)\right\},$$

where K_{pi} is penalty cost coefficient for over-generation of i-th wind farm; $f_w(W)$ is probability density function of wind power output; W_{iav} is available wind power.

The cost function of the i-th wind farm, designed to account for under-generation by engaging reservists, is given as follows [4]

$$C_{rwi}(W_i - W_{iav}) = K_{ri}(W_i - W_{iav}) = K_{pi}\left\{(W - W_i) f_w(W)\right\},$$

where K_{ri} is reserve cost coefficient for under-generation of i-th wind farm.

Therefore, the overall cost function for the wind farm is

$$C_{wi}(W_i) = C_{pwi}(W_{iav} - W_i) + C_{rwi}(W_i - W_{iav}).$$

1.2.1 Constraints

The total real power generation by each generating unit must balance the predicted real power demand plus the real power losses

$$\sum_{i=1}^{NG} P_{gi} \sum_{i=1}^{NB} P_{oi} - P_L = 0,$$

where P_{oi} is active power demand on the i-th bus; NB is number of buses; P_L is real power losses.

Similarly, for reactive power

$$\sum_{i=1}^{NG} Q_{gi} - \sum_{i=1}^{NB} Q_{oi} - Q_L = 0,$$

where Q_{oi} is reactive power demand on the i-th bus; NB is number of buses; NG is number of generators, and Q_L is reactive losses.

Active and reactive power operating limit (generation capacity limits) is given by

$$P_{gi}^{\min} \le P_{gi} \le P_{gi}^{\max} \quad (i=1, 2\ldots NG),$$

where $P_{gi}^{\min}$ and $P_{gi}^{\max}$ are the minimum and maximum limits for active power generation by i-th unit.

The power balance constraints to be satisfied for thermal and wind energy are

– Real power balance constraints

$$\sum_{i=1}^{NG} P_{gi} + \sum_{i=1}^{NW} P_{wi} - \sum_{i=1}^{NB} P_{Di} - \sum P_L = 0;$$

– Reactive power balance constraints

$$\sum_{i=1}^{NG} Q_{gi} + \sum_{i=1}^{NW} Q_{wi} - \sum_{i=1}^{NB} Q_{Di} - \sum Q_L = 0,$$

where P_{Di} and Q_{Di} are drawn active and reactive power; while P_{wi} and Q_{wi} are the active and reactive wind power.

1.3 Algorithm

The algorithm for determining real and reactive power participation factors is addressed in this section. Real power participation factors are formulated for general distributed generators, while the reactive power slack is allocated using a distributed slack model within the Newton-Raphson method. The NR method is preferred for the distributed slack bus model due to several advantages over the Gauss-Seidel method:

1. It exhibits a rapid convergence rate, necessitating fewer iterations to reach a solution.

2. Its performance is not influenced by the number of buses in the system, making it suitable for large-scale practical applications.

3. The convergence of this method remains unaffected by the choice of slack bus, allowing for flexibility in slack bus distribution.

4. It provides greater accuracy and reliability, particularly in large systems.

In contrast, the Gauss-Seidel and Fast Decoupled methods are inherently disqualified for power flow analysis in the DSB model, as they are sensitive to the slack bus's location. The Newton-Raphson method, being insensitive to the slack bus position, emerges as the optimal choice for power flow analysis in the DSB model.

1.3.1 Distributed slack bus algorithm based on real power participation factors

The distributed slack bus selected based on real power generator output participation factors is implemented using a NR solver. The selected algorithm is illustrated below.

Step 1: Read system data and formulate Y_{bus}.

Step 2: Initialize bus voltage magnitudes $|V_i|$, phase angles δ and set initial P_{loss}=0.

Step 3: Set iteration counter K=0 and convergence criteria ε.

Step 4: Set initial values of P_{gi} and determine initial participation factor K_i^0.

Step 5: Compute $P_i^{(k)}$ and $Q_i^{(k)}$ for system buses using the equations:

$$P_i = \sum_{k=1}^{n} |V_i| \cdot |V_k| \cdot |Y_{ik}| \cos(\theta_{ik} + \delta_k - \delta_i) + K_i \cdot P_{loss}, \quad Q_i = -\sum_{k=1}^{n} |V_i| \cdot |V_k| \cdot |Y_{ik}| \sin(\theta_{ik} + \delta_k - \delta_i).$$

Step 6: Compute residuals $\Delta P_i^{(k)}$ and $\Delta Q_i^{(k)}$.

Step 7: Compute largest of absolute residues of P_i and Q_i between two successive iterations:
– if residue < ε: STOP;

– if not, Compute elements of the extended Jacobian (J_e) where $J_e = \frac{dF}{dx}$ for each iteration.

Step 8: Solve for $J_e^{(k)}\Delta x^{(k)} = -F^{(k)}$.

Step 9: Update values of V_i, δ_i and P_{loss} for the next iteration i.e. $x^{(k+1)} = x^{(k)} + \Delta x^{(k)}$.

Step 10: Let K=K+1.

Step 11: Check real and reactive limits of the participating generators. If it violates the limits, we change it into a constant PQ injection, increment the counter and go to step 4.

Step 12: If generator limits are not violated, we then calculate the participation factor K_i and go to step 5.

1.3.2 Distributed slack bus algorithm based on reactive power participation factors

The distributed slack bus selected based on real power generator output participation factors is implemented using a NR solver as shown above. A distributed slack bus algorithm based on reactive power participation factors is developed in this paper as follows:

Step 1: Read system data and formulate Y_{bus}.

Step 2: Initialize bus voltage magnitudes $|V_i|$, phase angles δ and set initial Q_{loss}=0.

Step 3: Set iteration counter K=0 and convergence criteria ε.

Step 4: Set initial values of Q_{gi} and determine initial reactive power participation factor K_t^0.

Step 5: Compute $P_i^{(k)}$ and $Q_i^{(k)}$ for system buses using the equations:

$$P_i = \sum_{k=1}^{n} |V_i| \cdot |V_k| \cdot |Y_{ik}| \cos(\theta_{ik} + \delta_k - \delta_i), \quad Q_i = -\sum_{k=1}^{n} |V_i| \cdot |V_k| \cdot |Y_{ik}| \sin(\theta_{ik} + \delta_k - \delta_i) + K_t \cdot P_{loss}.$$

Step 6: Compute residuals $\Delta P_i^{(k)}$ and $\Delta Q_i^{(k)}$.

Step 7: Compute largest of absolute residues of P_i and Q_i between two successive iterations:
– if residue < ε: STOP;

– if not, Compute elements of the extended Jacobian (J_e) where $J_e = \frac{dF}{dx}$ for each iteration.

Step 8: Solve for $Je^{(k)}\Delta x^{(k)} = -F^{(k)}$.

Step 9: Update values of V_i, δ_i and Q_{loss} for the next iteration i.e. $x^{(k+1)} = x^{(k)} + \Delta x^{(k)}$.

Step 10: Let K=K+1.

Step 11: Check real and reactive limits of the participating generators. If it violates the limits, we change it into a constant PQ injection, increment the counter and go to step 4.

Step 12: If generator limits are not violated, we then calculate the participation factor K_t and go to step 5.

1.4 Flow charts

Fig. 1 shows flow chart of the distributed slack bus algorithm.

2 Results and analysis

2.1 Case study

2.1.1 IEEE 14 Bus Test Network

A one-line diagram for the test network is shown Fig. 2.

In the context of the distributed slack bus, Bus 1 is designated as a PV bus. Table 1 presents the bus data for the IEEE 14 bus test network, while Table 2 and Table 3 provide the line data and cost coefficients for the same network, respectively.

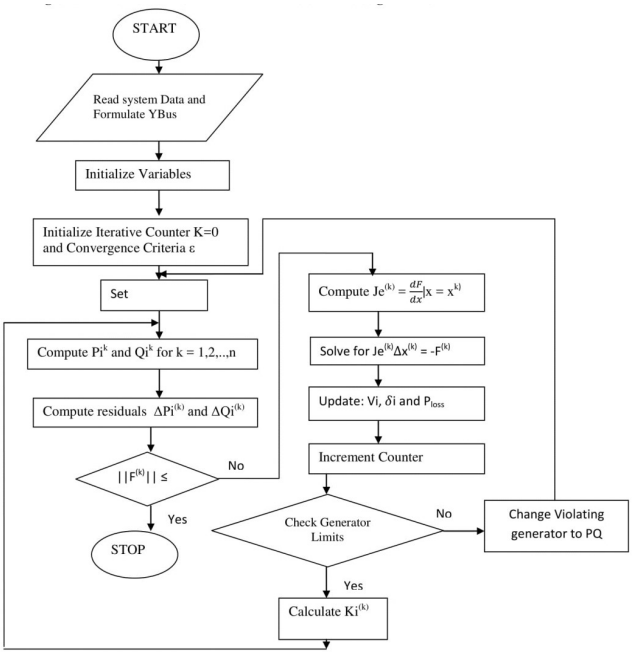

Fig. 1 Flow chart of the distributed slack bus

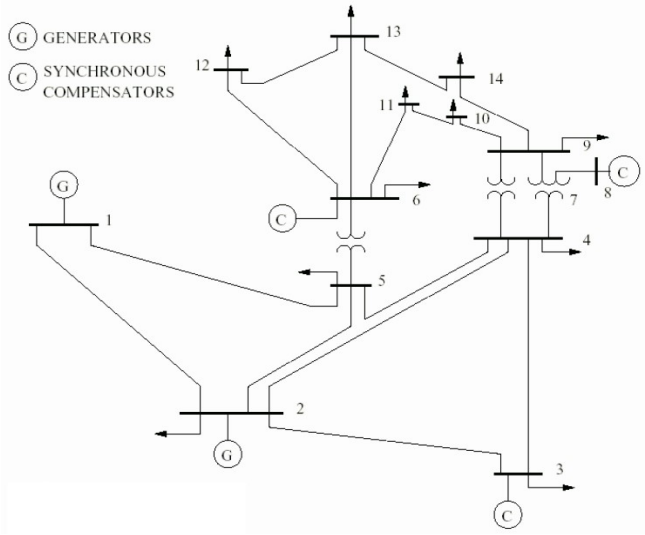

Fig. 2 IEEE 14 bus test network

Table 1. Bus data for IEEE 14 bus test network

Bus	Type	Specified voltage	Angle	Real power gen, MW	Reactive power gen, MVar	Load P_1, MW	Load Q_1, MVar	Q^{min}	Q^{max}
1	SLAC	1.060	0	232.4	-16.9	0.0	0.0	0	0
2	PV	1.045	0	40.0	42.4	21.7	12.7	-40	50
3	PV	1.010	0	0.0	23.4	94.2	19.0	0	0
4	PQ	1.000	0	0.0	0.0	47.8	-3.9	0	0
5	PQ	1.000	0	0.0	0.0	7.6	1.6	0	0
6	PV	1.070	0	0.0	12.2	11.2	7.5	-6	24
7	PQ	1.000	0	0.0	0.0	0.0	0.0	0	0
8	PV	1.090	0	0.0	17.4	0.0	0.0	-6	24
9	PQ	1.000	0	0.0	0.0	29.5	16.6	0	0
10	PQ	1.000	0	0.0	0.0	9.0	5.8	0	0
11	PQ	1.000	0	0.0	0.0	3.5	1.8	0	0
12	PQ	1.000	0	0.0	0.0	6.1	1.6	0	0
13	PQ	1.000	0	0.0	0.0	13.5	5.8	0	0
14	PQ	1.000	0	0.0	0.0	14.90	5.0	0	0

Table 2. Line data for IEEE 14 bus test network

From Bus	To Bus	Resistance, p.u.	Reactance, p.u.	Half-line susceptance ($B/2$)	Transformer tap settings
1	2	0.01938	0.05917	0.0264	1
2	3	0.04699	0.19797	0.0219	1
2	4	0.05811	0.17632	0.0187	1
1	5	0.05403	0.22304	0.0246	1
2	5	0.05695	0.17388	0.0173	1
3	4	0.06701	0.17103	0.0064	1
4	5	0.01335	0.04211	0	1
5	6	0	0.25202	0	0.932
4	7	0	0.20912	0	0.978
7	8	0	0.17615	0	1.000
4	9	0	0.55618	0	0.969
7	9	0	0.11001	0	1
9	10	0.03181	0.08450	0	1
6	11	0.09498	0.19890	0	1
6	12	0.12291	0.25581	0	1
6	13	0.06615	0.13027	0	1
9	14	0.12711	0.27038	0	1
10	11	0.08205	0.19207	0	1
12	13	0.22092	0.19988	0	1
13	14	0.17093	0.34802	0	1

Table 3. Cost coefficients for IEEE 14 bus

Gen no.	a_i, \$/MWhr	b_i, \$/MWhr	c_i, \$/hr
1	0.0430293	20	100
2	0.25	20	70
3	0.01	40	100
4	0.01	40	70
5	0.01	40	40

2.2 Results and validation

2.2.1 IEEE 14 bus results

2.2.1.1 Ordinary NR using single slack bus

Table 4 shows IEEE 14 bus output data with single slack bus, while Table 5 shows IEEE 14 bus line flows and losses with single slack bus.

Table 4. IEEE 14 bus output data with single slack bus

Bus no.	V, p.u.	Angle	P_G	Q_G	P_L	Q_L	P_I	Q_I
1	1.0600	0.0000	232.593	-15.233	0	0	232.593	-15.233
2	1.0450	-4.9890	40.000	47.928	21.7	12.7	18.300	35.228
3	1.0100	-12.7487	0	27.758	94.2	19.0	-94.200	8.758
4	1.0133	-10.2429	0	0	47.8	-3.9	-47.800	3.900
5	1.0166	-8.7606	0	0	7.6	1.6	-7.600	-1.600
6	1.0700	-14.4470	0	0	11.2	7.5	-11.200	15.526
7	1.0457	-13.2375	0	23.026	0	0	0	0
8	1.0800	-13.2375	0	0	0	0	0	21.030
9	1.0306	-14.8207	0	21.030	29.5	16.6	-29.500	-16.600
10	1.0299	-15.0365	0	0	9.0	5.8	-9.000	-5.800
11	1.0461	-14.8584	0	0	3.5	1.8	-3.500	-1.800
12	1.0533	-15.2974	0	0	6.1	1.6	-6.100	-1.600
13	1.0466	-14.2814	0	0	13.5	5.8	-13.500	-5.800
14	1.0193	-16.0721	0	0	14.9	5.0	-14.900	-5.000
Total			**272.593**	**104.509**	**259.0**	**73.5**	**13.593**	**31.009**

Generation cost: single slack bus (SSB) thermal cost – 4814.131 $/Hr; SSB overall cost – 4781.009 $/Hr; convergence achieved after – 7 iterations.

Table 5. IEEE 14 bus line flows and losses with single slack bus

From–to	*P*, MW	*Q*, Mvar	From–To	*P*, MW	*Q*, Mvar	Loss, MW	Loss, Mvar
1–2	157.080	-17.484	2–1	-152.772	30.369	4.309	13.155
1–5	75.513	7.981	5–1	72.740	3.464	2.773	11.455
2–3	73.396	5.936	3–2	71.063	3.894	2.333	9.830
2–4	55.943	2.935	4–2	54.273	2.132	1.670	5.067
2–5	41.733	4.738	5–2	40.813	-1.929	0.920	2.890
3–4	-23.137	7.752	4–3	23.528	-6.753	0.391	0.998
4–5	-59.585	11.574	5–4	60.064	-10.063	0.479	1.511
4–7	27.066	-15.396	7–4	-27.066	17.372	0	1.932
4–9	15.464	-2.640	9–4	15.464	3.932	0	1.292
5–6	45.889	-20.843	6–5	-45.889	26.617	0	5.774
6–11	8.287	8.898	11–6	-8.165	-8.641	0.123	0.257
6–12	8.064	3.176	12–6	-7.9485	-3.008	0.081	0.168
6–13	18.337	9.981	13–6	-18.085	-9.485	0.252	0.496
7–8	0	-20.362	8–7	0	21.030	0	0.668
7–9	27.066	14.798	9–7	-27.066	-13.840	0	0.957
9–10	4.393	-0.904	10–9	-4.387	0.920	0.006	0.016
9–14	8.637	0.321	14–9	-8.547	-0.131	0.089	0.190
10–11	-4.613	-6.720	11–10	4.665	6.841	0.051	0.120
12–13	1.884	1.408	13–12	-1.873	-1.398	0.011	0.001
13–14	6.458	5.083	14–13	-6.353	-4.869	0.105	0.215
Total loss						**13.593**	**56.910**

2.2.1.2 IEEE 14 bus distributed slack bus model

Table 6 presents the bus output data with a distributed slack bus using real power factor. Table 7 illustrates the line flows and losses of the IEEE 14 bus system, also employing a distributed slack bus and utilizing real power factor. In contrast, Table 8 and Table 9 display the bus output data of the IEEE 14 bus using reactive power factor, along with the respective line flows and losses with a distributed slack bus for reactive power factor.

Table 6. IEEE 14 bus output data with distributed slack bus using real power factor

Bus no.	*V*, p.u.	Angle	P_G	Q_G	P_L	Q_L	P_I	Q_I
1	1.0700	11.8713	232.408	6.325	0	0	232.408	6.325
2	1.0450	7.1139	40.001	27.802	21.7	12.7	18.301	15.102
3	1.0100	-0.6377	0	27.037	94.2	19.0	-94.200	8.037
4	1.0144	1.8474	0	0	47.8	-3.9	-47.800	3.900
5	1.0186	3.3143	0	0	7.6	1.6	-7.600	-1.600
6	1.0700	-2.3537	0	21.944	11.2	7.5	-11.200	14.444
7	1.0462	-1.1461	0	0	0	0	0	0
8	1.0800	-1.1461	0	20.695	0	0	0	20.695
9	1.0311	-2.7297	0	0	29.5	16.6	-29.500	-16.600
10	1.0304	-2.9452	0	0	9.0	5.8	-9.000	-5.800
11	1.0464	-2.7663	0	0	3.5	1.8	-3.500	-1.800
12	1.0533	-3.2039	0	0	6.1	1.6	-6.100	-1.600
13	1.0467	-3.2385	0	0	13.5	5.8	-13.500	-5.800
14	1.0196	-3.9797	0	0	14.9	5.0	-14.900	-5.000
Total			**272.409**	**103.803**	**259.0**	**73.5**	**13.409**	**30.303**

Table 7. IEEE 14 bus line flows and losses with distributed slack bus using real power factor

From–to	*P*, MW	*P*, MW	From–to	*P*, MW	*P*, MW	Loss, MW	Loss, Mvar
1–2	156.840	0.349	2–1	-152.677	12.364	4.164	12.713
2–3	75.567	11.815	3–2	-72.807	-0.419	2.761	11.397
2–4	73.320	5.944	4–2	-70.991	3.866	2.328	9.810
1–5	55.924	2.243	5–1	-54.257	2.815	1.667	5.058
2–5	41.735	3.572	5–2	-40.820	-0.778	0.915	2.794
3–4	-23.209	7.058	4–3	23.595	-6.071	0.387	0.987
4–5	-59.725	9.739	5–4	60.200	-8.241	0.475	1.499
5–6	27.100	-15.087	6–5	-27.100	16.999	0	1.912
4–7	15.487	-2.515	7–4	-15.487	3.804	0	1.289
7–8	45.827	-20.042	8–7	-45.827	25.706	0	5.664
4–9	8.253	8.793	9–4	-8.132	-8.541	0.121	0.253
7–9	8.057	3.163	9–7	-7.976	-2.996	0.080	0.167
9–10	18.317	9.927	10–9	-18.066	-9.433	0.251	0.494
6–11	0	-20.049	11–6	0	20.695	0	0.647
6–12	27.100	14.825	12–6	-27.100	-13.866	0	0.959
6–13	4.424	-0.807	13–6	-4.418	0.823	0.006	0.016
9–14	8.662	0.384	14–9	-8.572	-0.192	0.090	0.191
10–11	-4.582	-6.623	11–10	4.632	6.741	0.050	0.117
12–13	1.876	1.396	13–12	-1.865	-1.386	0.011	0.010
13–14	6.432	5.019	14–13	-6.328	-4.808	0.104	0.211
Total loss						**13.409**	**56.187**

Generation cost: DSB thermal cost – 4801.906; DSB overall cost – 4768.870; convergence achieved after – 6 iterations.

Table 8. IEEE 14 bus output data with distributed slack bus using reactive power factor

Bus no.	*V*, p.u.	Angle	P_G	Q_G	P_L	Q_L	P_I	Q_I
1	1.0500	12.0665	223.861	-35.774	0	0	223.861	-35.774
2	1.0450	7.0834	46.150	57.193	21.7	12.7	24.450	44.493
3	1.0200	-0.6686	2.287	37.215	94.2	19.0	-91.913	18.215
4	1.0142	1.8161	-1.790	-5.224	47.8	-3.9	-49.590	-1.324
5	1.0172	3.3072	2.114	-0.211	7.6	1.6	-5.486	1.811
6	1.0800	-2.3425	7.030	40.454	11.2	7.5	-4.170	32.954
7	1.0503	-1.1766	0	-5.963	0	0	0	-5.963
8	1.1000	-1.1738	0.032	31.006	0	0	0.032	31.006
9	1.0337	-2.7573	0	0	29.5	16.6	-29.500	-16.600
10	1.0326	-2.9662	0	0	9.0	5.8	-9.000	-5.800
11	1.0475	-2.7727	-2.080	-4.273	3.5	1.8	-5.580	-6.073
12	1.0535	-3.1932	-1.657	-3.322	6.1	1.6	-7.757	-4.922
13	1.0471	-3.2329	-3.344	-6.339	13.5	5.8	-16.844	-12.139
14	1.0213	-3.9896	0	0	14.9	5.0	-14.900	-5.000
Total			**272.603**	**104.762**	**259.0**	**73.5**	**13.603**	**31.262**

Table 9. IEEE 14 bus line flows and losses with distributed slack bus for reactive power factor

From–to	*P*, MW	*Q*, Mvar	From–to	*P*, MW	*Q*, Mvar	Loss, MW	Loss, Mvar
1–2	150.170	-33.304	2–1	-146.011	46.002	4.159	12.698
2–3	73.691	3.152	3–2	-71.025	7.853	2.666	11.006
2–4	72.822	0.832	4–2	-70.540	8.783	2.282	9.615
1–5	55.951	2.328	5–1	-54.282	2.736	1.669	5.063
2–5	41.689	4.351	5–2	-40.772	-1.554	0.916	2.797
3–4	-21.374	12.377	4–3	21.767	-11.374	0.393	1.003
4–5	-59.781	12.541	5–4	60.265	-11.014	0.484	1.527
5–6	27.194	-17.195	6–5	-27.194	19.253	0	2.058
4–7	15.512	-3.045	7–4	-15.512	4.354	0	1.309
7–8	46.047	-24.905	8–7	-46.047	31.125	0	6.221
4–9	10.349	12.729	9–4	-10.130	-12.270	0.219	0.459
7–9	9.751	6.551	9–7	-9.606	-6.248	0.145	0.303
9–10	21.776	16.317	10–9	-21.356	-15.490	0.420	0.827
6–11	-0.032	-29.606	11–6	0.032	31.006	0	1.400
6–12	27.226	16.257	12–6	-27.226	-15.254	0	1.003
6–13	4.501	-0.278	13–6	-4.495	0.294	0.006	0.016
9–14	8.737	0.724	14–9	-8.646	-0.529	0.091	0.194
10–11	-4.505	-6.094	11–10	4.550	6.197	0.044	0.103
12–13	1.849	1.327	13–12	-1.839	-1.317	0.010	0.009
13–14	6.351	4.668	14–13	-6.254	-4.471	0.097	0.197
Total loss						**13.603**	**57.809**

Generation cost: DSB reactive with renewable energy cost – 757.623 $/Hr; DSB reactive thermal cost – 834.150 $/Hr; convergence achieved after – 4 iterations.

Therefore, the total cost is: DSB with renewable energy using combined power factor (thermal) –

$$(4801.906 \cdot 0.8) + (834.150 \cdot 0.2) = 4008.3548 \text{ \$/Hr};$$

DSB with renewable energy using combined power factor (with renewable energy):

$$(4768.870 \cdot 0.8) + (757.623 \cdot 0.2) = 3966.6206 \text{ \$/Hr}.$$

2.3 Analysis and discussion

Table 10 and Table 11 show comparison of generated real power, and comparison of generation costs, respectively.

Fig. 3 and Fig. 4 show the voltage profile comparison, and voltage angle comparison.

Table 10. Comparison of generated real power

		SSB model, MW	DSB using real power factor, MW	DSB using reactive power factor, MW
Generation	Plant 1	232.593	232.408	223.861
	Plant 2	40.000	40.001	46.150
Total system losses		13.593	13.409	13.603

Table 11. Comparison of generation costs

	SSB model	DSB model with real power factor	DSB model with combined power factor
Generation cost for thermal generators, $/hr	4814.131	4801.906	4008.3548
Generation cost for thermal & renewable energy generators, $/hr	4781.009	4768.870	3966.6206

It can be observed from Fig. 3 that the voltage magnitudes across the buses exhibit a high degree of similarity. In contrast, the voltage angles display considerable variation between the two models, as illustrated in Fig. 4. In the SSB model, bus 1 serves as the reference bus, assigned a phase angle of 0. Conversely, the DSB model allocates system mismatches among all PV buses through participation factors, leading to

alterations in phase angles. The DSB model achieves a reduction in power losses by 0.184 MW when utilizing real power participation factors in comparison to the SSB model. However, the DSB model does not yield any improvement in losses when reactive power participation factors are employed, as reactive power signifies the energy absorbed by the system. The real power outputs from generators in the DSB model are marginally lower than those in the SSB model, as shown in Table 10. This results in a decreased generation cost in the DSB model, as evidenced in Table 11. The integration of renewable energy contributes to a reduction in generation costs for both the SSB and DSB models, as indicated in Table 11.

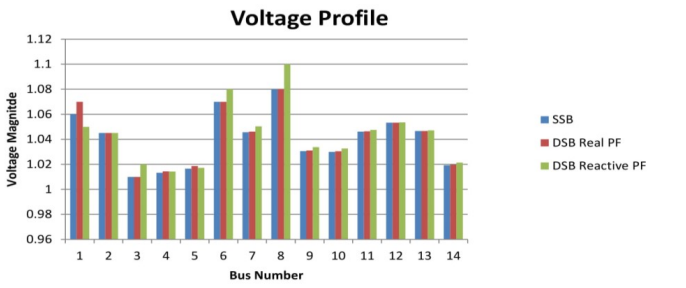

Fig. 3. Voltage profile comparison

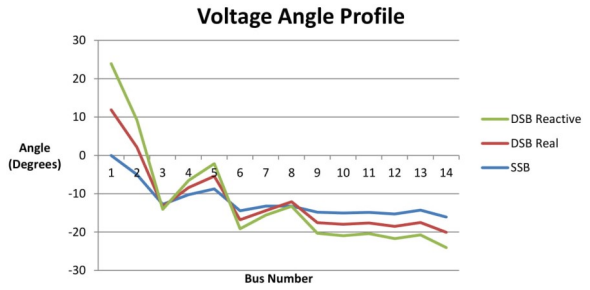

Fig. 4. Voltage angle comparison

Conclusion

The investigation of SSB modeling for distribution power flow analysis has been conducted. Initially, the distribution power flow using a DSB modelwas examined. Subsequently, scalar participation factors were employed to allocate uncertain real and reactive power system losses for three-phase power flow computations. Furthermore, renewable energy sources, such as wind and solar generators, were integrated into the system as distributed generators, and the generation costs were compared to those of a system devoid of renewable energy. The DSB approach offered a more realistic framework for power system analysis compared to the SSB, proving to be a superior technique for deregulated distributed generation systems that incorporate renewable energy. The DSB effectively distributes system losses, enabling dispersed generators to adjust their outputs to satisfy the load and loss demands of the network. This is accomplished through the application of participation factors and combined participation factors based on generation capacity. The developed algorithm has demonstrated robustness and is suitable for implementation in larger systems. The DSB can be utilized in various applications, including capacitor placement and sizing, network reconfiguration, distributed system expansion, and service restoration.

References

1. Billy, O. (2015). Distributed slack bus for economic dispatch of renewable energy. Graduation Project, University of Nairobi, Kenya.
2. Vural, A. M. (2015). Interior point-based slack-bus free-power flow solution for balanced islanded microgrids. *International Transactions on Electrical Energy Systems*, vol. 26, iss. 5, pp. 968–992. https://doi.org/10.1002/etep.2117.
3. Ortega, J., Molina, T., Muñoz, J. C., & Oliva H., S. (2020). Distributed slack bus model formulation for the holomorphic embedding load flow method. *Transactions on Electrical Energy Systems*, vol. 30, iss. 3. https://doi.org/10.1002/2050-7038.12253.
4. Gautam, M., Bhusal, N., Thapa, J., & Benidris, M. (2022). A cooperative game theory-based approach to formulation of distributed slack buses. *Sustainable Energy, Grids and Networks*, vol. 32, article 100890. https://doi.org/10.1016/j.segan.2022.100890.
5. Huang, Y., Sun, Q., Wang, R., & Liu, G. L. (2023). A network-based virtual slack bus model for energy conversion units in dynamic energy flow analysis. *Science China Technological Sciences*, vol. 66, pp. 243–254. https://doi.org/10.1007/s11431-022-2172-8.
6. Huang, Y., Sun, Q., Zhang, N., & Wang, R. (2024). A multi-slack bus model for bi-directional energy flow analysis of integrated power-gas systems. *CSEE Journal of Power and Energy Systems*, vol. 10, no. 5, pp. 2186–2196. https://doi.org/10.17775/CSEEJPES.2020.04190.
7. Huang, Y., Ding, T., Mu, C., Zhang, X., He, Y., & Shahidehpour, M. (2024). Distributed slack-bus based DC optimal power flow with transmission loss: A second-order cone programming approach and sufficient condi-

tions. *IEEE Transactions on Automation Science and Engineering*, vol. 21, no. 3, pp. 3873–3885. https://doi.org/10.1109/TASE.2023.3289306.

Received 19 May 2025
Accepted 30 June 2025

Розробка системи відновлюваної енергії з використанням моделі розподіленої балансуючої шини

M. Al-Rawi

Бандунгський технологічний інститут,
Jalan Ganesa No. 10, Coblong, Kota Bandung, Jawa Barat, 40132, Індонезія

У цьому дослідженні розроблено підхід з використанням розподіленої балансуючої шини (РБШ), що враховує комбіновані коефіцієнти участі, засновані на запланованих генеруючих потужностях системи для розподілу втрат системи між генераторами. Алгоритм РБШ було створено та реалізовано з використанням алгоритму Ньютона-Рафсона в середовищі MATLAB. Як приклад дослідження використана 14-шинна система IEEE. В систему інтегровано відновлювані джерела енергії, та проведено порівняльний аналіз витрат на генерацію між системами, що включають відновлювані джерела енергії, та системами, що використовують тільки теплові генератори, з використанням моделі з однією балансуючою шиною, так і моделі РБШ. Впровадження розподіленого балансування вузлів призвело до зниження загального вироблення активної електроенергії з 272,593 МВт до 272,409 МВт у системі з 14 вузлами, а також до зниження собівартості виробництва електроенергії на обох типах вузлів. Крім того, було мінімізовано втрати активної потужності в лініях електропередачі. Зміни рівнів вироблення електроенергії на вузлах з регульованою напругою сприяли створенню ефективної схеми економічної диспетчеризації, що точно відображає параметри мережі. Впровадження вітрових та сонячних електростанцій значно знизило собівартість виробництва електроенергії порівняно з системами, які не використовують ці ресурси. Більше того, використання комбінованих коефіцієнтів участі дозволило отримати ще більш точну мережеву модель.

***Ключові слова**: розподілена балансуюча шина, відновлювана енергія, економічна диспетчеризація, електроенергія.*

Література

1. Billy O. Distributed slack bus for economic dispatch of renewable energy. Graduation Project, University of Nairobi, Kenya, 2015.
2. Vural A. M. Interior point-based slack-bus free-power flow solution for balanced islanded microgrids. *International Transactions on Electrical Energy Systems*. 2015. Vol. 26. Iss. 5. P. 968–992. https://doi.org/10.1002/etep.2117.
3. Ortega J., Molina T., Muñoz J. C., Oliva H. S. Distributed slack bus model formulation for the holomorphic embedding load flow method. *Transactions on Electrical Energy Systems*. 2020. Vol. 30. Iss. 3. https://doi.org/10.1002/2050-7038.12253.
4. Gautam M., Bhusal N., Thapa J., Benidris M. A cooperative game theory-based approach to formulation of distributed slack buses. *Sustainable Energy, Grids and Networks*. 2022. Vol. 32. Article 100890. https://doi.org/10.1016/j.segan.2022.100890.
5. Huang Y., Sun Q., Wang R., Liu G. L. A network-based virtual slack bus model for energy conversion units in dynamic energy flow analysis. *Science China Technological Sciences*. 2023. Vol. 66. P. 243–254. https://doi.org/10.1007/s11431-022-2172-8.
6. Huang Y., Sun Q., Zhang N., Wang R. A multi-slack bus model for bi-directional energy flow analysis of integrated power-gas systems. *CSEE Journal of Power and Energy Systems*. 2024. Vol. 10. No. 5. P. 2186–2196. https://doi.org/10.17775/CSEEJPES.2020.04190.
7. Huang Y., Ding T., Mu C., Zhang X., He Y., Shahidehpour M. Distributed slack-bus based DC optimal power flow with transmission loss: A second-order cone programming approach and sufficient conditions. *IEEE Transactions on Automation Science and Engineering*. 2024. Vol. 21. No. 3. P. 3873–3885. https://doi.org/10.1109/TASE.2023.3289306.